Case Studies in Construction Materials 22 (2025) e04193

Contents lists available at ScienceDirect

Case Studies in Construction Materials

journal homepage: www.elsevier.com/locate/cscm

Studies on the mechanical properties of interlayer interlocking 3D printed concrete based on a novel nozzle

Youbao Jiang [a], Pengxiang Gao [a], Sondipon Adhikari [b], Xiaofei Yao [c], Hao Zhou [a,d,*], Yan Liu [a]

[a] School of Civil Engineering, Changsha University of Science & Technology, Changsha 410114, China
[b] James Watt School of Engineering, The University of Glasgow, G12 8QQ, UK
[c] CCCC First Highway Consultants Co., Ltd., Xi'an 710075, China
[d] Engineering Research Center of Catastrophic Prophylaxis and Treatment of Road & Traffic Safety of Ministry of Education, Changsha University of Science & Technology, Changsha, 410114, Hunan, China

ARTICLE INFO

Keywords:
3D printed concrete
Interlayer interlocking
Mechanical properties
Failure mode
Anisotropic behavior

ABSTRACT

The interlocking can effectively improve the mechanical properties of concrete. However, the strength of 3D printed concrete with interlocking interfaces, fabricated using non-automated methods, is reduced due to the time-consuming interface processing. Additionally, studies on the effects of interlocking on the mechanical properties, failure modes, and anisotropic behavior of 3D printed concrete are not yet systematic. In order to address these issues, a printing forming scheme and nozzles were designed for interlayer interlocking 3D printing, and the mechanical properties of interlayer interlocking 3D printed concrete were tested. Firstly, the forming scheme and nozzles are specifically designed for the preparation of 3D printed concrete with interlocking interfaces between the layers. Furthermore, extrudability tests are carried out to determine the appropriate printing parameters for interlayer interlocking 3D printed concrete. Finally, specimens were printed, and interfacial splitting tests, interlayer interfacial shear tests, and compression tests were conducted. The results reveal that: (1) by utilizing the appropriate extrusion rate of the rotating shaft and nozzle travel speed, better-formed interlayer interlocking concrete filaments can be obtained. (2) the interlayer interlocking 3D printed specimens exhibit higher strength. The interfacial splitting tensile strength is increased by about 14.5–30.7 %, and the interlayer interfacial shear strength is increased by about 7.8–18.0 % compared to those with smooth interlayer interfaces. (3) the interlayer interlocking 3D printed concrete exhibits a reduction in the anisotropic coefficient of about 13.7–25.5 %, and the anisotropy is significantly weakened.

1. Introduction

Currently, the optimized design of structures is receiving increasing attention [1], and the 3D printed concrete technology can realize the accurate forming of these structures. Additionally, this technology offers high efficiency, intelligence, and reduced formwork usage [2]. In recent years, there has been a significant amount of research on several aspects of 3D printed concrete, such as

---

* Corresponding author at: School of Civil Engineering, Changsha University of Science & Technology, Changsha 410114, China.
E-mail address: zhouhao@csust.edu.cn (H. Zhou).

https://doi.org/10.1016/j.cscm.2024.e04193
Received 29 September 2024; Received in revised form 14 December 2024; Accepted 30 December 2024

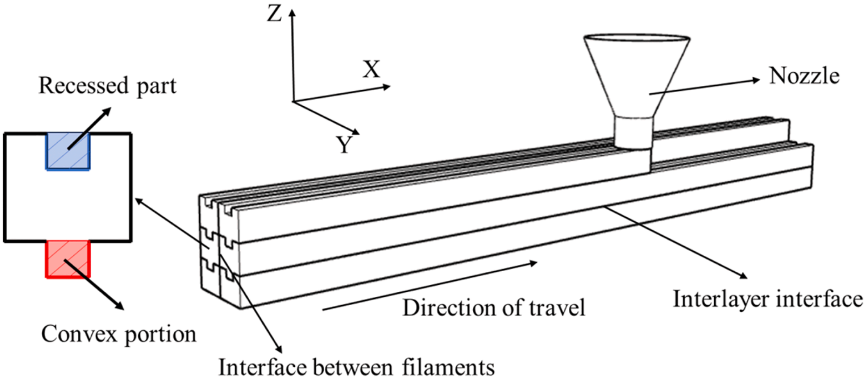

Fig. 1. Forming scheme of interlayer interlocking 3D printed concrete.

materials and workability [3,4], printing parameters and paths [5,6], the performance of 3D printed structures [7,8], and the construction of complex structures [9,10]. Moreover, the mechanical properties of 3D printed concrete have been a hot topic [11,12].

The interfaces created during the deposition of concrete filaments affect the mechanical properties of 3D printed concrete. Specifically, the strength of 3D printed concrete decreases and exhibits anisotropy [13,14]. In addition, the loading direction corresponding to the maximum strength is not consistently determined [15,16]. To improve the mechanical properties of 3D printed concrete, scholars have summarized the results of mechanical properties tests on 3D printed concrete and analyzed the reasons for variations in strength under different loading directions [17].

Some researchers have investigated 3D printed concrete with different components and optimized the material composition and process parameters to enhance the strength of 3D printed concrete. Ding et al. [18] examined the mechanical properties of 3D printed concrete with recycled sand and analyzed the anisotropy of compressive and flexural strengths. Moreover, the workability and mechanical properties of 3D printed concrete with other components have been explored, such as lightweight aggregate [19], nanosilica [20], and E6-glass fiber [21]. Jia et al. [22] investigated the impact of limestone powder on the mechanical properties of 3DP-UHPC, with test results demonstrating that the inclusion of 10 % limestone powder can enhance the flexural strength of 3DP-UHPC. In terms of the printing process, Panda et al. [23] demonstrated that reducing the distance of the nozzle to the model or increasing the travel speed can improve the interlayer tensile strength of 3D printed concrete. In addition, a proper curing environment [24] and an optimized printing path [25] can enhance the mechanical properties of 3D printed concrete. To achieve concrete filaments with improved mechanical properties, Xu et al. [26] investigated the effect of the combination of nozzle travel speed and volumetric flow rate on the printed quality. In terms of nozzle design, concrete filaments extruded through a rectangular nozzle exhibit better shape stability and higher mechanical strength than those extruded through a round nozzle [27]. Some researchers have also designed nozzles with side blades [28] to further enhance the shape stability of concrete filaments and the overall performance of 3D printed concrete.

Interlocking has been widely used in various fields [29,30]. In addition, interlocking can enhance the mechanical properties of the bond interface in cast-in-place concrete [31]. Scholars are interested in fully utilizing the advantages of interlocking to obtain 3D printed concrete with higher mechanical properties. Zareiyan et al. [32] conducted a study on the mechanical properties of 3D printed concrete with interlocking interfaces and smooth interfaces. The results showed that specimens with interlocking interfaces had enhanced splitting tensile strength and compressive strength. In another study, He et al. [33] tested the mechanical properties of 3D printed specimens. The results showed that 3D printed concrete with serrated interlayer interfaces exhibited higher interlayer tensile strength and interlayer shear strength. Wang et al. [34] improved the bonding between prefabricated 3D printed concrete parts using different adhesives and interlocking geometries and tested the mechanical properties of the concrete specimens. Qiu et al. [35] found that the grooved and 3D-printed interface effectively enhanced the interfacial bond between 3DP UHP-SHCC permanent formwork and post cast normal concrete. Putten et al. [36] constructed the interlocking interface using a device with combs and investigated the related mechanical properties.

It can be determined that 3D printed concrete with interlocking interfaces exhibits higher mechanical properties compared to that with smooth interfaces. Moreover, the interfacial strength of 3D printed concrete with interlocking interfaces is significantly improved. However, there are few studies on the interlayer interlocking 3D printed concrete forming process. Some studies used non-automated methods [32,36] to construct the interlocking interface between the layers. Further research is needed to understand the mechanical properties, failure modes, and anisotropic behavior of interlayer interlocking 3D printed concrete. In this paper, the dimensions of the interlocking nozzles are designed and a forming scheme is proposed. Furthermore, extrudability tests are carried out to determine the printing parameters for interlayer interlocking 3D printed concrete. Finally, specimens are printed and interfacial splitting tests, interlayer interfacial shear tests, and compression tests are conducted.

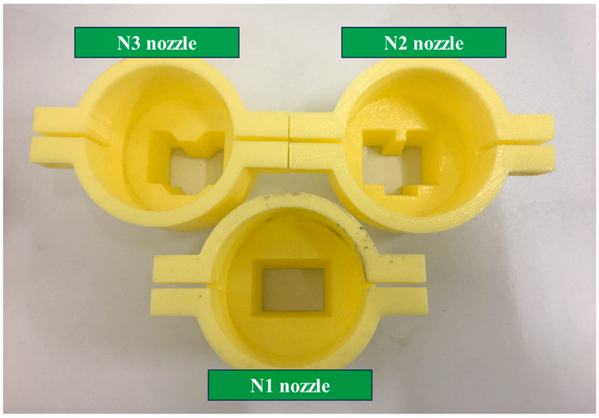

(a) Interlayer interlocking nozzles.

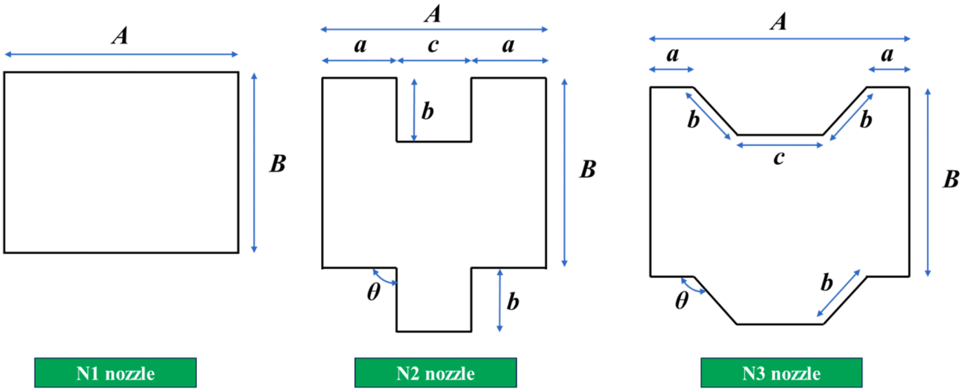

(b) Dimension parameters of the nozzle extrusion outlet.

Fig. 2. Design of interlayer interlocking nozzles.

Table 1
Dimension parameters of the interlayer interlocking nozzles.

Nozzle	S_N/mm^2	ξ	k	θ/°	A/mm	B/mm	a/mm	b/mm	c/mm
N1	600	1.5	1/4	-	30	20	-	-	-
N2	600	1.5	1/4	90	30	20	10	5	10
N3	600	1.5	1/4	135	30	20	5	7.07	10

2. Forming of interlayer interlocking 3D printed concrete

2.1. Forming scheme

In 3D printed concrete technology, the material is extruded through a nozzle and deposited layer by layer. The extruded material can maintain a certain geometric shape that is closely related to the geometry of the extrusion outlet of the nozzle [4,21]. This means that by designing extrusion outlets with different shapes, it is possible to print concrete filaments in various forms. However, adjustments to material ratios, printing paths, and printing parameters are also necessary. In this paper, in order to realize the printing of 3D printed concrete with interlocking interfaces, the forming scheme (Fig. 1) and nozzles are designed. The preparation of interlayer interlocking 3D printed specimens is achieved through the direct extrusion and deposition of concrete filaments with interlocking surfaces.

2.2. Design of nozzles

In this paper, nozzles that can directly extrude concrete filaments with interlocking surfaces are referred to as interlocking nozzles. When these interlocking surfaces are positioned between layers, these nozzles will be referred to as interlayer interlocking nozzles. The

Table 2
Compositions of cementitious materials.

Material	OPC	R·SAC	Fly ash	Metakaolin	Silica fume
Weight (%)	71	4	10	10	5

Table 3
Mix ratio of 3D printed concrete (by weight).

Mix	Cementitious materials	Water	FS	PP Fiber	Superplasticizer
Ratio	100	25	80	0.30	0.35

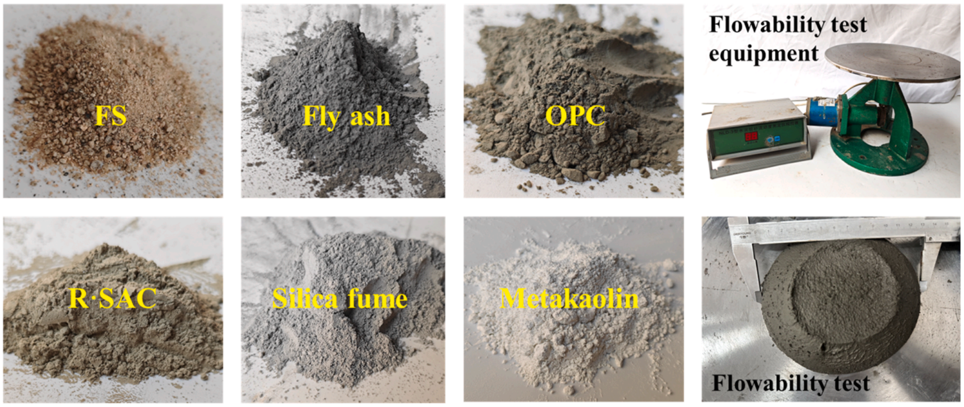

Fig. 3. Material and flowability test.

interlayer interlocking nozzles have an extrusion outlet with a tooth-like cross-section, as depicted in Fig. 2. The extrusion channel is sloped, creating a pre-forming environment for the concrete.

Based on the related studies [37–40], and the team's research results, the dimensions of the extrusion outlet of the interlayer interlocking nozzles were determined, as shown in Table 1. The extrusion outlet length A is 30 mm, the extrusion outlet width B is 20 mm, the extrusion outlet area S_N is 600 mm^2, and the aspect ratio of the nozzle extrusion outlet ξ is 1.5. The dimension ratio k is defined by Eq. (1) in this paper. The dimension parameters for Eq. (1) are illustrated in Fig. 2(b).

$$k = b\sin(\pi - \theta)/B \tag{1}$$

The dimension ratio k is 1/4. The N1 nozzle is a square nozzle. The N2 nozzle has a tooth angle θ of 90°, while the N3 nozzle has a tooth angle θ of 135°.

3. Material Mix ratio and printing parameters

3.1. Material Mix ratio

The material mix ratio, as shown in Table 2 and Table 3, included ordinary Portland cement (OPC 42.5) and rapid hardening sulphoaluminate cement (R·SAC 42.5). Mineral admixtures such as fly ash, metakaolin, and silica fume were also added. Polypropylene fiber measuring 12 mm in length and 18 μm in diameter was used. Additionally, powdered naphthalene-based superplasticizer was included as part of the printable materials. To prevent nozzle blockage, fine sand with a fineness modulus ranging from 2.2 to 1.6 and an average grain size of 0.35–0.25 mm was selected.

The material and flowability test is shown in Fig. 3. The flowability test of 3D printed concrete was carried out in accordance with the Chinese standard GB/T 2419–2005 [41]. The samples were prepared using the mix ratio outlined in Table 2 and Table 3. The spreading diameter of the 3D printed concrete ranges from 131 mm to 140 mm.

3.2. Printing parameters

3.2.1. Printing parameters test scheme

In the extrudability test, the ability of the concrete to be continuously and stably extruded from the nozzle can be observed directly. By testing the quality of filament forming and filament width at different printing parameters, the better interlayer interlocking printing parameters can be determined. In this test, concrete filaments of 600 mm in length were printed using N2 and N3 nozzles,

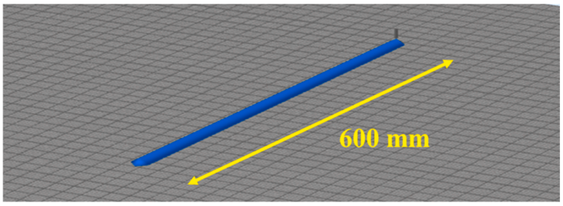

(a) Printed model.

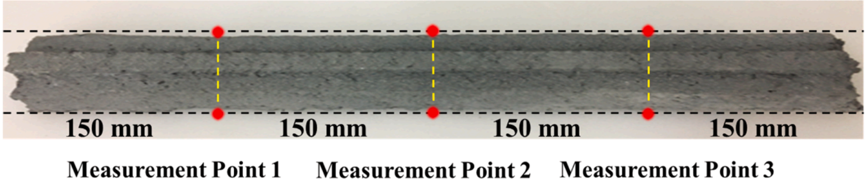

(b) Measurement points selection.

Fig. 4. Printing parameters test scheme.

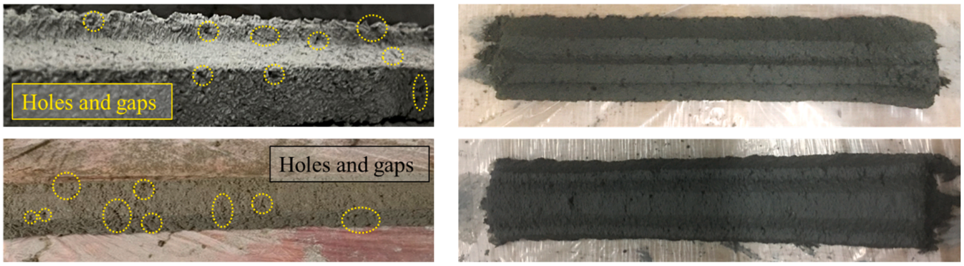

(a) Poorly forming.

(b) Better forming.

Fig. 5. Results of extrudability test.

Table 4
Filament widths with N2 nozzle at different travel speeds.

Nozzle travel speed/ (mm/s)	W_1/mm	W_2/mm	W_3/mm	W_{avg}/mm	δ/mm	Width change rate
10	37.22	37.15	37.07	37.15	7.15	23.8 %
20	35.24	34.98	34.75	34.99	4.99	16.6 %
30	32.72	33.30	34.63	33.55	3.55	11.8 %
40	30.85	30.41	29.49	30.25	0.25	0.8 %
50	26.71	25.67	26.18	26.19	−3.81	−12.7 %

respectively. The printed model is shown in Fig. 4(a). Three measurement points are taken at equal intervals along the filament, as illustrated in Fig. 4(b).

Printing parameters, such as the distance of the nozzle to the model, nozzle travel speed, and extrusion rate of the rotating shaft, greatly affect the quality of the concrete filament forming. The distance of the nozzle to the model was determined as 20 mm, based on nozzle design theory [42]. Following the team's established methodology [43,44], the extrusion rate of the rotating shaft was set at 1 r/s, while the nozzle travel speed was varied to print interlayer interlocking concrete filaments. The quality of the concrete filament forming was observed, and the widths of the filaments after stabilization were recorded. The filament widths at three measurement points, denoted as W_1, W_2, and W_3, were recorded. The width variation value (δ) was calculated according to Eq. 2.

$$\delta = W_{avg} - A \tag{2}$$

where W_{avg} is the average value of W_1, W_2, and W_3, δ is the value of filament width variation, and A is the nozzle extrusion outlet length.

3.2.2. *Results of printing parameters test*

The extrusion rate of the rotating shaft was set at 1 r/s, and the interlayer interlocking concrete filaments were printed using nozzle

Table 5
Filament widths with N3 nozzle at different travel speeds.

Nozzle travel speed/ (mm/s)	W_1/mm	W_2/mm	W_3/mm	W_{avg}/mm	δ/mm	Width change rate
10	38.18	37.24	37.12	37.51	7.51	25.0 %
20	36.25	34.63	35.38	35.42	5.42	18.1 %
30	33.25	33.17	32.63	33.02	3.02	10.1 %
40	31.86	31.78	31.72	31.79	1.79	6.0 %
50	26.59	25.88	26.32	26.26	−3.74	−12.5 %

Fig. 6. Concrete filaments.

Table 6
Overview of specimens.

Test （Dimension of specimen）	Loading direction	Number of specimens	Group
Interfacial splitting test （100 mm × 100 mm × 100 mm）	-	3 （Splitting test）	N0
	X	3	N1, N2, N3
	Y	3	N1, N2, N3
	Z	3	N1, N2, N3
Compression test （100 mm × 100 mm × 100 mm）	-	3	N0
	X	3	N1, N2, N3
	Y	3	N1, N2, N3
	Z	3	N1, N2, N3
Interlayer interfacial shear test （100 mm × 100 mm × 300 mm）	-	3 （Shear test）	N0
	Y	3	N1, N2, N3

travel speeds of 10 mm/s, 20 mm/s, 30 mm/s, 40 mm/s, and 50 mm/s. The test results are shown in Fig. 5. The filament widths with N2 and N3 nozzles are recorded in Table 4 and Table 5, respectively.

The test results show that polygonal extrusion outlets have more corners compared to round and square extrusion outlets. When the nozzle travel speed is faster, there is a higher likelihood of printing defects such as holes and gaps on the edges or surfaces of the interlayer interlocking concrete filament. To ensure good filament forming quality, it is recommended to select the nozzle travel speed within a 15 % change in filament width. In this study, the distance of the nozzle to the model is 20 mm, the extrusion rate of the rotating shaft is 1 r/s, and the nozzle travel speed is 30 mm/s. The concrete filaments were printed using these printing parameters with N1, N2, and N3 nozzles, as shown in Fig. 6.

4. Mechanical properties of interlayer interlocking 3D printed concrete

4.1. Specimen preparation

The number of 3D printed specimens and the loading direction are presented in Table 6. N1, N2, and N3 group specimens were printed using N1, N2, and N3 nozzles, respectively. For the interfacial splitting test and compression test, cubic specimens measuring 100 mm on each side were utilized. In the interlayer interfacial shear test, rectangular specimens with dimensions of 100 mm × 100 mm × 300 mm were used. N0 group specimens were cast-in-place specimens. The cast-in-place specimens were prepared in accordance with the Chinese standard GB/T50081–2019 [45]. These cast-in-place specimens used the same materials and dimensions as the 3D printed specimens.

The specimens were obtained by cutting the 3D printed concrete models using a rock cutter. The rectangular models were printed,

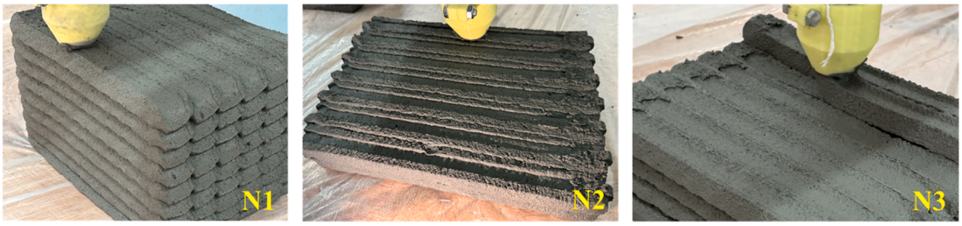

Fig. 7. Printing process.

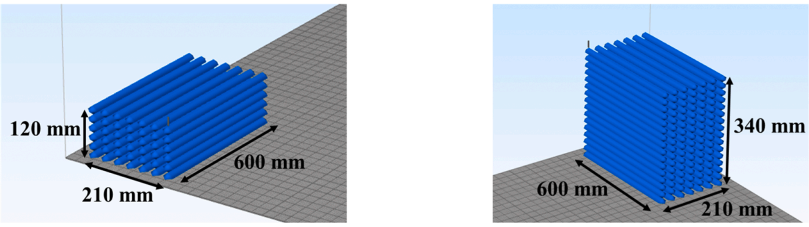

(a) Printed model (600 mm × 210 mm × 120 mm). (b) Printed model (600 mm × 210 mm × 340 mm).

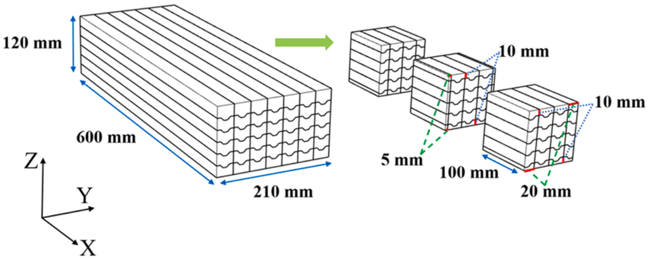

(c)Cutting scheme (600 mm × 210 mm × 120 mm).

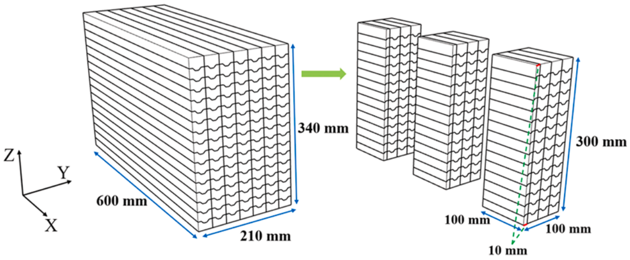

(d) Cutting scheme (600 mm × 210 mm × 340 mm).

Fig. 8. Printed models and cutting schemes.

as shown in Fig. 7. The printed models are shown in Fig. 8(a) and Fig. 8(b). Once the printing process was finished, the models were covered in plastic film. After seven days of maintenance, the 3D printed concrete models were cut. The cutting schemes are shown in Fig. 8(c) and Fig. 8(d). Before and after cutting, the models and the specimens were placed in an environment with a temperature of 20 ± 2 °C and a relative humidity of 95 ± 5 % for 28 days.

4.2. *Testing method*

4.2.1. *Interfacial splitting test*

Based on the Chinese standard [45], the interfacial splitting test was carried out using a servo-hydraulic universal testing machine. The loading rate is 0.05 MPa/s, and the test setup is shown in Fig. 9(a). In the loading scheme of the X and Y directions interfacial splitting test (Fig. 9(b) and Fig. 9(c)), the load is applied along the interlayer interface. In the Z direction loading scheme (Fig. 9(d)), the load is applied along the interface between filaments.

The interfacial splitting tensile strength of interlayer interlocking 3D printed concrete was calculated according to Eq. (3).

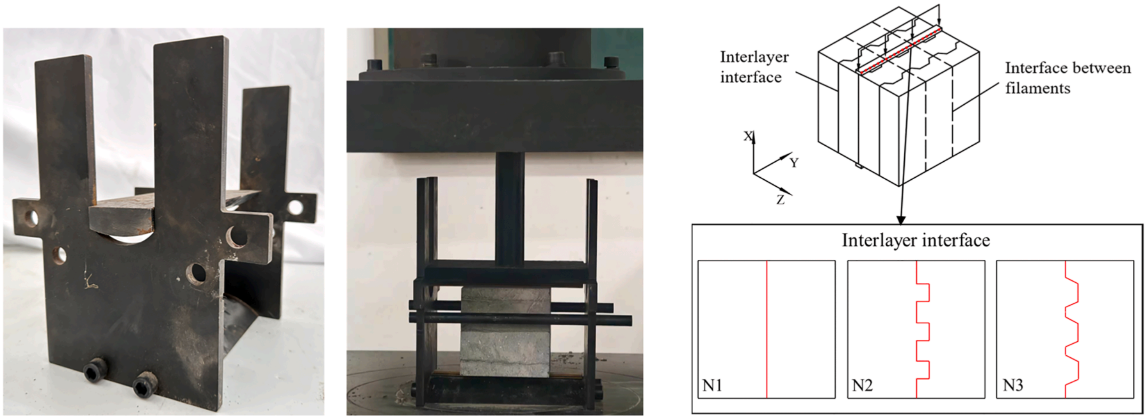

(a) Test setup. (b) X direction.

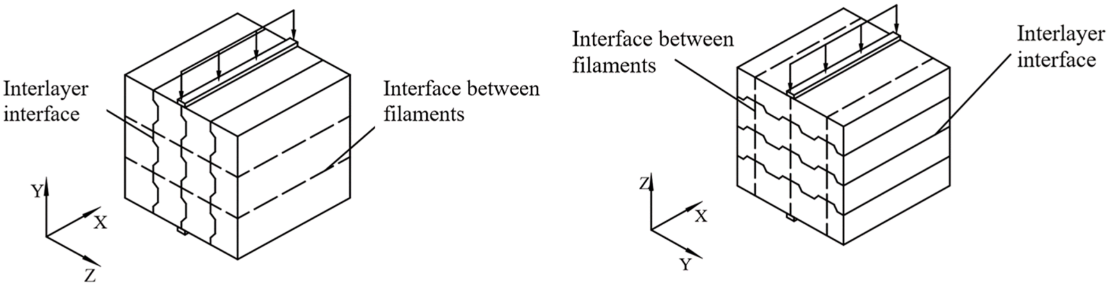

(c) Y direction. (d) Z direction.

Fig. 9. Interfacial splitting test.

$$f_{ts} = \frac{2F}{\pi S} = 0.637\frac{F}{S} \tag{3}$$

where f_{ts} is the interfacial splitting tensile strength of 3D printed concrete (MPa), F is the specimen failure load (N) in the interfacial splitting test, and S is the specimen splitting area (mm^2).

4.2.2. Interlayer interfacial shear test

According to the Chinese standard [46], the interlayer interfacial shear test was conducted using a servo-hydraulic universal testing machine. The loading rate is 0.06 mm/min. The loading scheme is shown in Fig. 10(a), and the test setup is shown in Fig. 10(b). The thickness of the steel bar, denoted as H, is 5 mm, which is less than 1/10 of the specimen section height h (h=100 mm). The spacing between the outer surfaces of the upper knife edges, denoted as L, is 100 mm. Additionally, the misalignment (α) between the upper and lower knife edges is within 1 mm.

The interlayer interfacial shear strength of interlayer interlocking 3D printed concrete was calculated according to Eq. (4).

$$f_v = \frac{F_v}{2b_s h} \tag{4}$$

where f_v is the interlayer interfacial shear strength of 3D printed concrete (MPa), F_v is the specimen failure load (N) in the interlayer interfacial shear test, b_s is the width of the specimen section (mm), and h is the height of the specimen section (mm).

4.2.3. Compression test

The compression test was conducted using a servo-hydraulic universal testing machine to determine the compressive strength of 3D printed concrete specimens. The load was applied along the X, Y, and Z directions, respectively. The loading scheme is illustrated in Fig. 11. The loading rate is 0.5 mm/min.

The compressive strength of interlayer interlocking 3D printed concrete was calculated according to Eq. (5).

$$f_c = \frac{F_c}{S_c} \tag{5}$$

where f_c is the compressive strength of 3D printed concrete (MPa), F_c is the specimen compressive failure load (N), and S_c is the

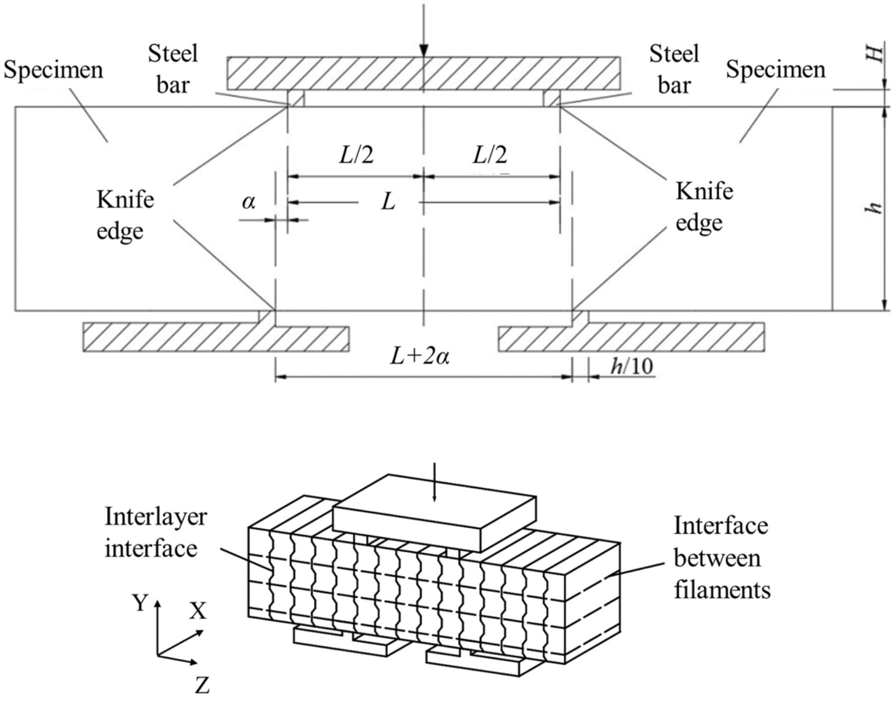

(a) Loading scheme.

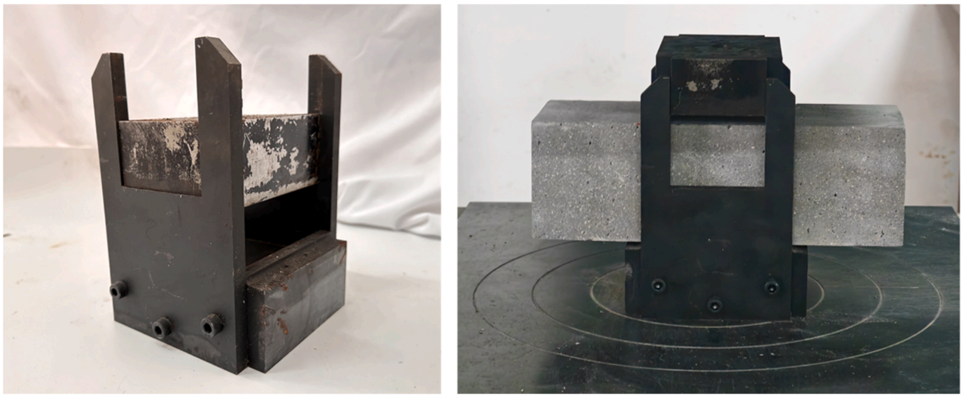

(b) Test setup.

Fig. 10. Interlayer interfacial shear test.

specimen compressive area (mm^2).

4.3. *Results of mechanical properties*

4.3.1. *Results of interfacial splitting test*

(1) Cast-in-place specimens

The cast-in-place specimens are denoted as the N0 test group, and the test results of the N0 group specimens are shown in Fig. 12.

(2) Interfacial splitting test (X direction)

The test results of 3D printed concrete specimens are illustrated in Fig. 13. In Fig. 13(a), it can be observed that the N1 group

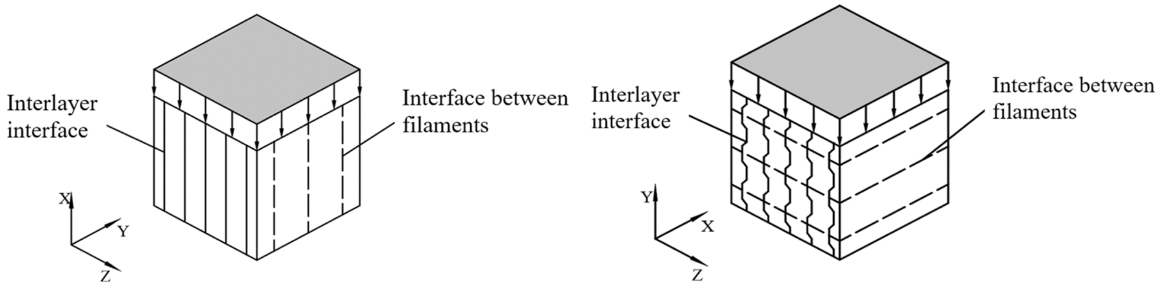

(a) X direction.

(b) Y direction.

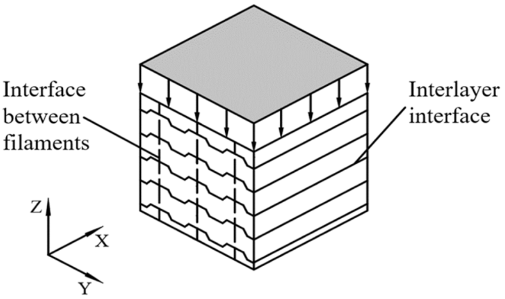

(c) Z direction.

Fig. 11. Loading scheme of compression test.

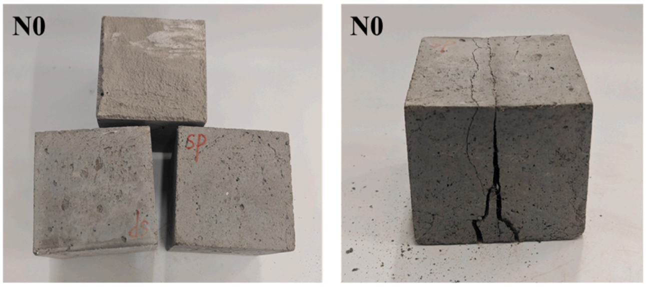

Fig. 12. Failure mode of cast-in-place specimens (N0).

specimens exhibit a failure mode similar to that of the N0 group specimens. Specifically, when the specimens were damaged, vertical through cracks appeared in the middle of the specimens. Additionally, a linear crack was present in the middle of the top surface of the specimens.

The failure modes of N2 and N3 group specimens are illustrated in Fig. 13(b) and Fig. 13(c), respectively. Vertical through cracks were observed in the middle of N2 and N3 group specimens. However, unlike the N0 and N1 group specimens, some of the cracks on the top surface of the N2 and N3 group specimens extended along the interlocking interface. On the fracture surfaces of the N2 and N3 group specimens, it is evident that a part of the concrete in the convex portion of the interlocking interface was damaged.

(3) Interfacial splitting test (Y direction)

In the Y-direction interfacial splitting test, vertical through cracks were observed in the middle of the specimens of the N1 group (Fig. 14(a)). However, specimens of the N2 and N3 groups exhibited cracks along the interlocking interface (Fig. 14(b) and Fig. 14(c)). Furthermore, the fracture surfaces of the specimens of the N2 and N3 groups show damage to the convex portion of the interlocking interface between the layers.

(4) Interfacial splitting test (Z direction)
    In the Z-direction interfacial splitting test, the failure modes of the 3D printed specimens were similar to those of the N0 group specimens. In addition, the ultimate loads of the specimens in groups N1, N2, and N3 were similar.
(5) Summary of interfacial splitting test

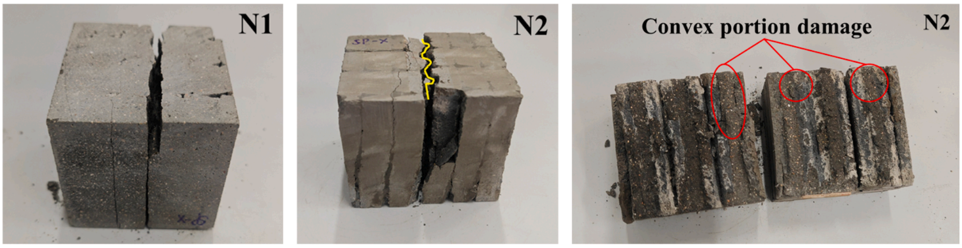

(a) N1. (b) N2.

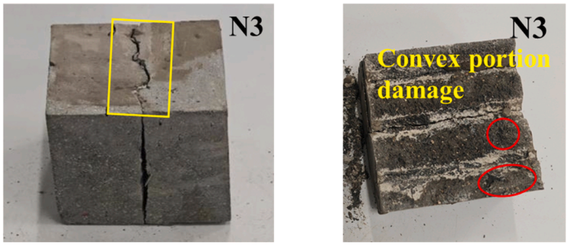

(c) N3.

Fig. 13. Failure mode of 3D printed concrete specimens (X direction).

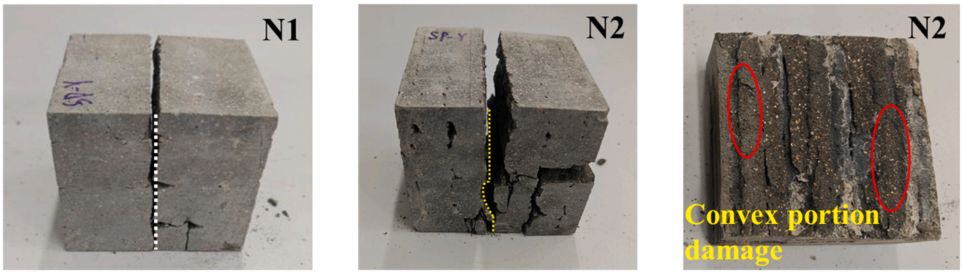

(a) N1. (b) N2.

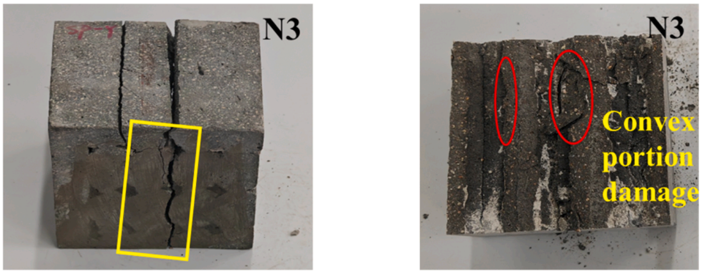

(c) N3.

Fig. 14. Failure mode of 3D printed concrete specimens (Y direction).

The splitting tensile strength of cast-in-place specimens (N0 group) is 6.27 MPa. The ultimate load and splitting tensile strength of 3D printed specimens in the test are recorded in Table 7, Table 8, and Table 9, respectively. The results of the interfacial splitting test are shown in Fig. 15.

The experimental results indicate that the interlayer interlocking 3D printed concrete with N2 and N3 nozzles exhibit higher interfacial splitting tensile strength in both the X and Y directions compared to that with the N1 nozzle. Specifically, the X-direction strength of the N2 group specimens increased by approximately 18.3 %, and the Y-direction strength increased by approximately

Table 7
X direction interfacial splitting tensile strength.

Group	Ultimate load /kN			Interfacial splitting tensile strength /MPa			Average /MPa
	1	2	3	1	2	3	
N1	59.58	52.34	55.26	3.80	3.33	3.52	3.55
N2	68.49	66.88	62.63	4.36	4.26	3.99	4.20
N3	73.49	70.58	74.21	4.68	4.50	4.73	4.64

Table 8
Y direction interfacial splitting tensile strength.

Group	Ultimate load /kN			Interfacial splitting tensile strength /MPa			Average /MPa
	1	2	3	1	2	3	
N1	57.65	58.32	56.28	3.67	3.71	3.59	3.66
N2	61.81	68.98	66.36	3.94	4.39	4.23	4.19
N3	73.92	73.15	72.64	4.71	4.66	4.63	4.67

Table 9
Z direction interfacial splitting tensile strength.

Group	Ultimate load /kN			Interfacial splitting tensile strength /MPa			Average /MPa
	1	2	3	1	2	3	
N1	44.00	52.02	48.59	2.80	3.31	3.10	3.07
N2	48.23	49.56	51.66	3.07	3.16	3.29	3.17
N3	52.35	46.95	48.24	3.33	2.99	3.07	3.13

14.5 %. The X-direction strength of the N3 group specimens increased by about 30.7 %, and the Y-direction strength increased by about 27.6 %. In contrast, the interfacial splitting tensile strength in the Z direction is relatively consistent, ranging from approximately 3.07 to 3.17 MPa.

3D printed specimens with a square nozzle yield pure adhesive failure in the interfacial splitting test [18,47]. However, the failure mode of 3D printed concrete with a tooth-like nozzle differs from that with the square nozzle. When the load is applied along the interlayer interface, some cracks extend along the interlocking interface. Additionally, the specimens with interlocking interfaces between the layers exhibit a mixed mode of cohesive and adhesive failures. It is important to note that both adhesive failure and the mixed failure mode may coexist on a concrete filament, as seen on the fracture surface of the interlayer interlocking 3D printed specimen.

The cohesive failure is considered to be the ideal failure mode of the specimen, usually correlated to the highest strength [48,49]. The experimental results demonstrated that the interlocking interface effectively enhanced the interfacial splitting tensile strength of 3D printed concrete. The strength in the X direction increased by approximately 18.3 %-30.7 %, while the strength in the Y direction increased by about 14.5 %-27.6 %. Additionally, when the load was applied along the Z direction, the strengths of the specimens were similar, indicating that the interlocking interface between the layers had less impact on the strength of the interface between the filaments. The splitting tensile strength and failure mode of the bilayer specimens were correlated with the notch depth as well as the tooth angle [32,33]. The test results revealed that a mixed failure mode occurred for both specimens with a tooth angle of 90° and a tooth angle of 135°, at a layer thickness of 20 mm and a notch depth of 5 mm. Furthermore, the specimens with a tooth angle of 135° exhibited higher strength in the X and Y directions compared to those with a tooth angle of 90°. According to the CT-scan images (Fig. 16), the filaments with a tooth angle of 90° may introduce more porosity during deposition, which reduces the strength of the specimens.

4.3.2. Results of interlayer interfacial shear test

In the shear test, Fig. 17 depicts the different failure modes of the specimens. Fig. 17(a) and Fig. 17(b) demonstrate that the N0 group specimen exhibits a fracture surface with an inclination angle, while the crack on the N1 group specimens extends along the interlayer interfaces. On the other hand, the failure modes of the specimens of the N2 and N3 groups differed from those of the N0 and N1 groups (Fig. 17(c) and Fig. 17(d)). Specifically, zigzag cracks appeared when the specimen was damaged.

The ultimate load and shear strength of specimens in the test are recorded in Table 10 and Table 11, respectively. The results of the interlayer interfacial shear test are shown in Fig. 18. The test results demonstrate that the interlocking interface can improve the interlayer interfacial shear strength of 3D printed concrete. The strength enhancement is approximately 7.8–18.0 % compared to the 3D printed specimens with smooth interlayer interfaces.

3D printed specimens with smooth interfaces yield pure adhesive failure in the interlayer interfacial shear test [50]. Beushausen [51] and Wu [52] conducted studies on the failure mode of concrete interfaces with notches under shear. While cohesive failure was observed in the N0 group specimens and pure adhesive failure was observed in the N1 group specimens, the interlayer interlocking 3D

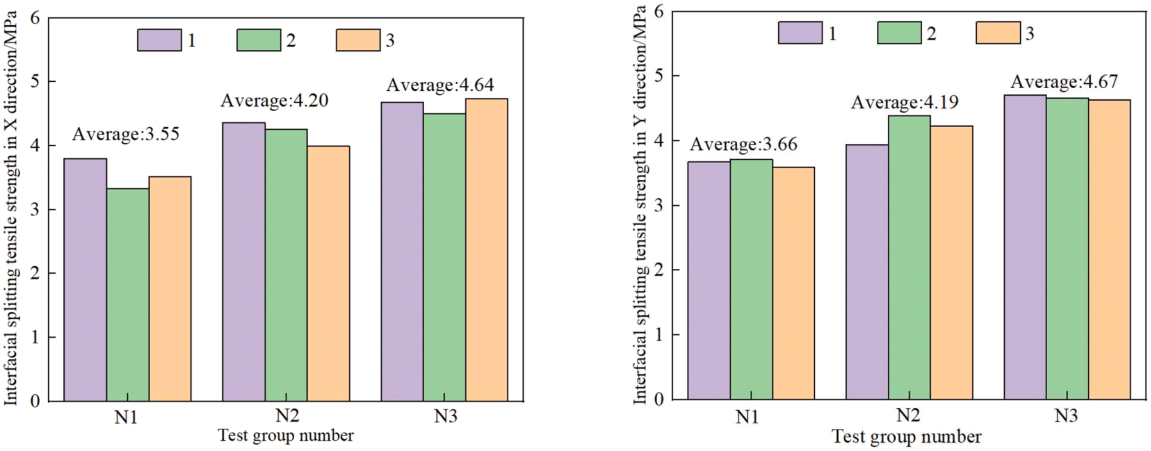

(a) Strength in the X direction.

(b) Strength in the Y direction.

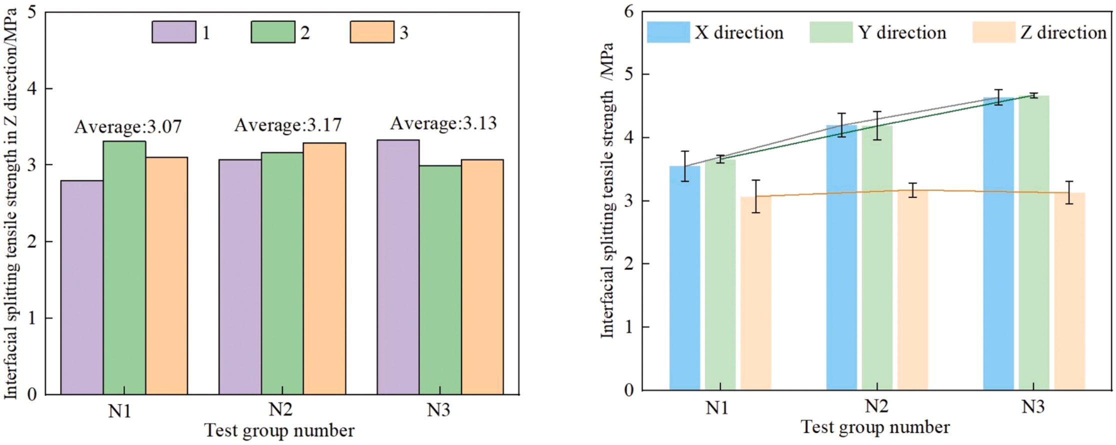

(c) Strength in the Z direction.

(d) Interfacial splitting tensile strength.

Fig. 15. Results of the interfacial splitting tensile strength.

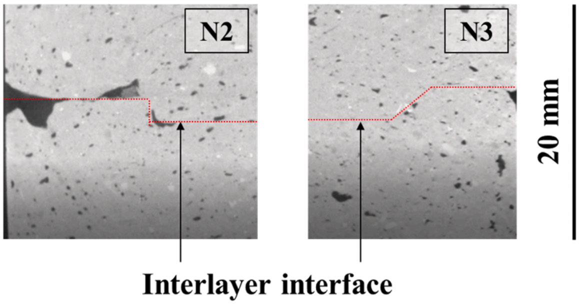

Fig. 16. CT-scan images of 3D printed specimens.

printed specimens exhibited a combination of cohesive and adhesive failures, resulting in the appearance of zigzag cracks.

The shear key angle [53] and the base area [54] have a significant impact on the shear strength of the specimens. The interlayer interfacial shear strength of the 3D printed specimen, with interlocking interfaces between the layers, increased by approximately 7.8–18.0 % compared to that of the N1 group specimens. Additionally, the strength of the N3 group specimens increased by about 9.4 % compared to that of the N2 group specimens. This suggests that the specimens with a tooth angle of 135° had a larger base area, which contributed to the improvement.

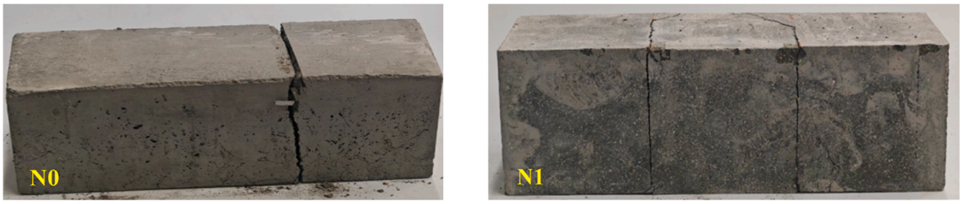

(a) N0. (b) N1.

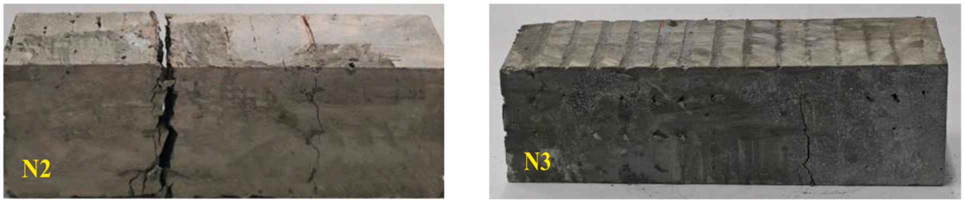

(c) N2. (d) N3.

Fig. 17. Failure mode of specimens (shear test).

Table 10
Shear strength of cast-in-place specimens.

Group	Ultimate load /kN			Shear strength /MPa			Average /MPa
	1	2	3	1	2	3	
N0	87.62	79.35	84.49	4.38	3.97	4.22	4.19

Table 11
Interlayer interfacial shear strength of specimens.

Group	Ultimate load /kN			Interlayer interfacial shear strength /MPa			Average /MPa
	1	2	3	1	2	3	
N1	60.41	50.51	65.75	3.02	2.53	3.29	2.95
N2	67.31	59.66	63.52	3.37	2.98	3.18	3.18
N3	68.96	71.58	68.30	3.45	3.58	3.42	3.48

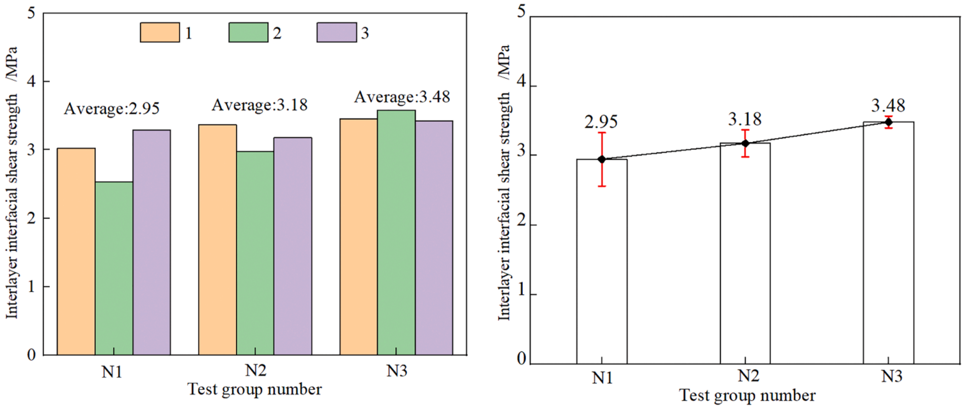

Fig. 18. Results of the interlayer interfacial shear strength.

4.3.3. Results of compression test

In the compression test, the failure modes of the specimens are shown in Fig. 19. The compressive strength of the specimens is recorded in Table 12. The results of the compression test are shown in Fig. 20.

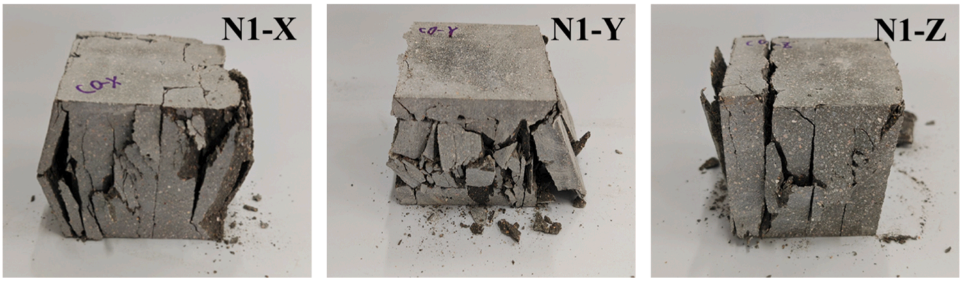

(a) N1.

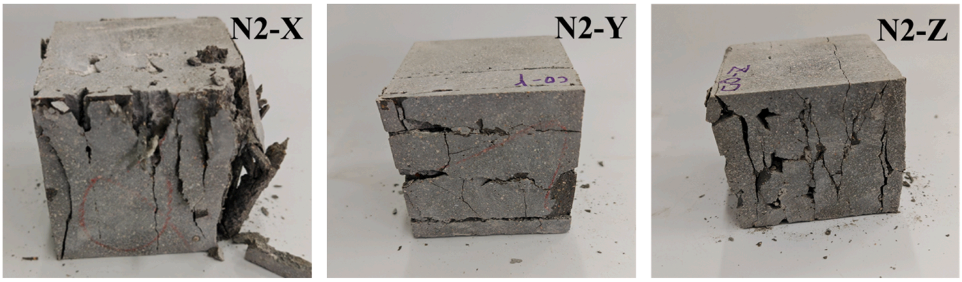

(b) N2.

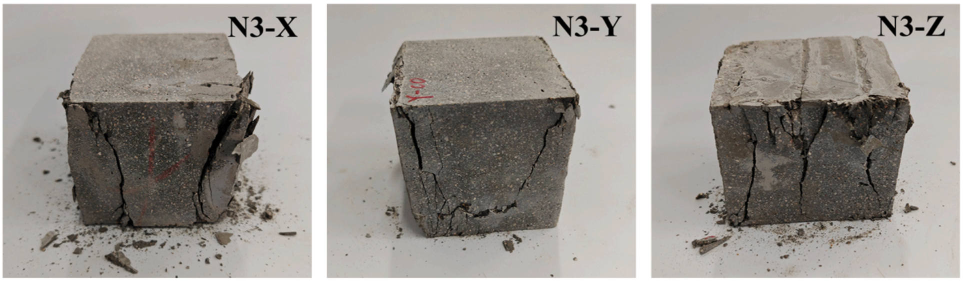

(c) N3.

Fig. 19. Failure mode of 3D printed specimens (compression test).

Table 12
Compressive strength of specimens.

Group	Compressive strength /MPa	Compressive strength in the X direction /MPa	Compressive strength in the Y direction /MPa	Compressive strength in the Z direction /MPa
N0	62.80	-	-	-
N1	-	47.03	37.34	35.37
N2	-	53.13	42.19	41.46
N3	-	53.88	44.21	40.65

As depicted in Fig. 19, the failure modes of the N2 and N3 groups specimens differed from those of the N1 group specimens. Specifically, the number of interfacial cracks is decreased and the degree of horizontal slip is reduced. Compared to the compressive strength of 3D printed concrete with a square nozzle, the interlayer interlocking 3D printed concrete demonstrated an increase of approximately 13.0–18.4 %. Moreover, the cracking load of the interlocking interface is enhanced compared to the smooth interface, resulting in an increased compressive strength of interlayer interlocking 3D printed concrete.

4.4. Mechanical anisotropy evaluation

The above test results show that the 3D printed specimens have significant anisotropic behavior. The anisotropic coefficient, I_a, was

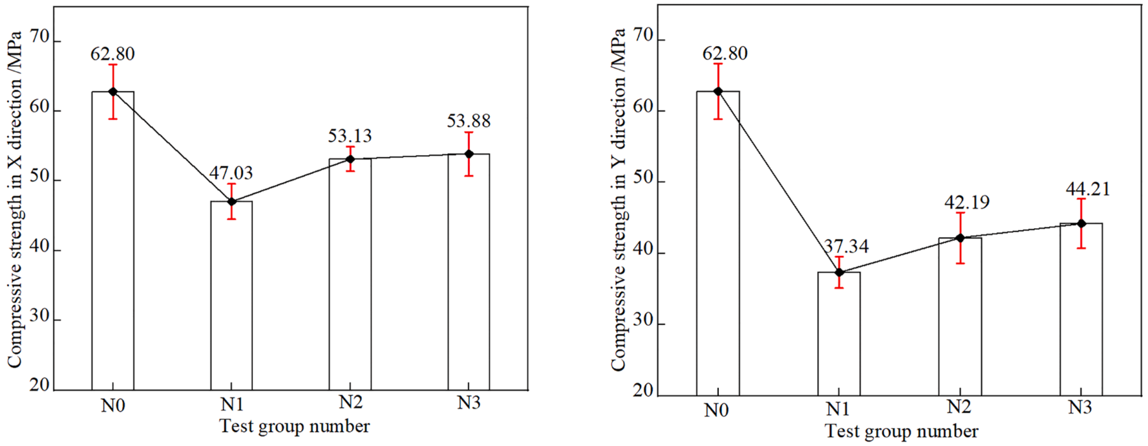

(a) Compressive strength in X direction. (b) Compressive strength in Y direction.

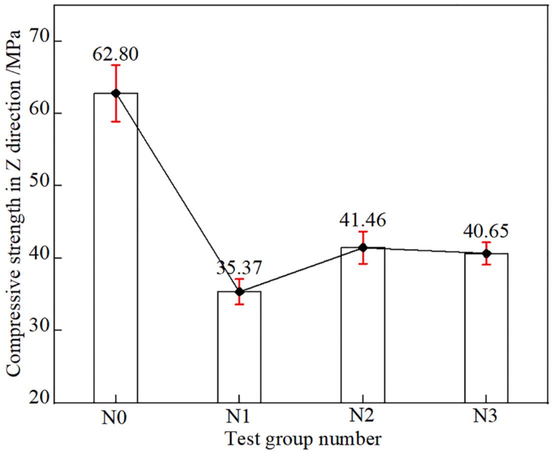

(c) Compressive strength in Z direction.

Fig. 20. Results of the compressive strength.

Table 13
Anisotropic coefficient of compressive strength.

Group	f_X /MPa	f_Y /MPa	f_Z /MPa	I_a
N0	-	-	-	0
N1	47.03	37.34	35.37	0.647
N2	53.13	42.19	41.46	0.497
N3	53.88	44.21	40.65	0.482

Table 14
Anisotropic coefficient of interfacial splitting tensile strength.

Group	f_X /MPa	f_Y /MPa	f_Z /MPa	I_a
N0	-	-	-	0
N1	3.55	3.66	3.07	0.789
N2	4.20	4.19	3.17	0.681
N3	4.64	4.67	3.13	0.619

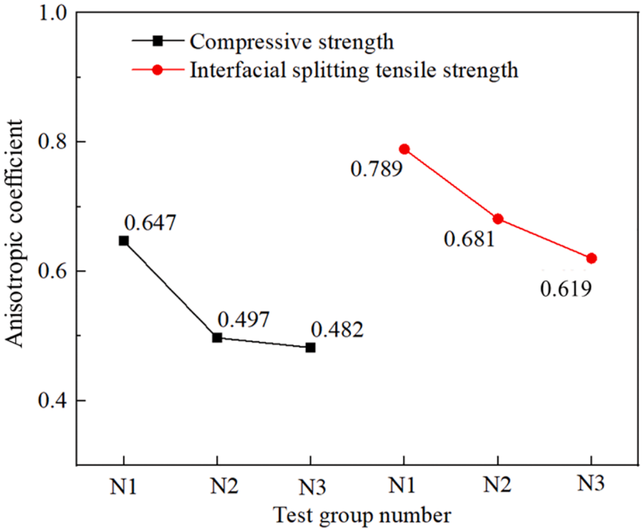

Fig. 21. Variation of the anisotropic coefficient.

used to describe the anisotropic behavior of the printed specimens [55]. I_a was calculated by Eq. (6).

$$I_a = \frac{\sqrt{(f_X - f_0)^2 + (f_Y - f_0)^2 + (f_Z - f_0)^2}}{f_0} \tag{6}$$

where f_X, f_Y, and f_Z are the strengths of the interlayer interlocking 3D printed concrete when loaded along the X, Y, and Z directions, respectively, and f_0 is the strength of the cast-in-place specimen. The cast-in-place specimen is treated as homogeneous material, and the I_a is equal to 0. The smaller the anisotropic coefficient, the weaker the anisotropy.

The compressive strength, interfacial splitting tensile strength, and corresponding anisotropic coefficient (I_a) of the 3D printed specimens are recorded in Table 13 and Table 14, respectively. The variation of the anisotropic coefficient (I_a) is shown in Fig. 21. The results indicate that the interlayer interlocking 3D printed concrete exhibits a reduction in the anisotropic coefficient (I_a) of about 13.7–25.5 %, resulting in weaker anisotropy compared to the 3D printed concrete with smooth interfaces.

The printing interlayer is a key factor that affects the mechanical anisotropy [20]. During compression tests, interlocking increased the cracking load of the interlayer interface, resulting in a decrease in the number of interfacial cracks. Furthermore, the degree of horizontal slip caused by interfacial cracking was reduced, leading to enhanced compressive strength. In the interfacial splitting test, a mixed mode of cohesive and adhesive failures appeared on the fracture surface of the interlayer interlocking 3D printed specimens. There was a significant improvement in the bonding of the interlayer interface. As a result, the anisotropy of the interlayer interlocking 3D printed concrete was weakened.

5. Conclusions

This study conducted extrudability tests to determine the appropriate printing parameters for the proposed forming scheme of interlayer interlocking 3D printed concrete. Additionally, compression tests, interfacial splitting tests, and interlayer interfacial shear tests were performed on the interlayer interlocking 3D printed specimens. The mechanical properties, failure modes, and anisotropy of the specimens were analyzed. The main conclusions are drawn as follows :

(1) By utilizing the appropriate extrusion rate of the rotating shaft and nozzle travel speed, better-formed interlayer interlocking concrete filaments can be obtained. These appropriate printing parameters can prevent the occurrence of holes or gaps on the edges or surfaces of the interlayer interlocking filaments.

(2) The interfacial splitting tensile strength of the 3D printed specimens, with interlocking interfaces between the layers, is increased by approximately 14.5 %-30.7 % compared to those with a square nozzle. Additionally, for the compactness and interfacial splitting tensile strength, the nozzle with a tooth angle of 135° is more advantageous.

(3) The interlayer interfacial shear strength of 3D printed concrete with interlocking interfaces is increased by approximately 7.8 %-18.0 % compared to the 3D printed specimens with smooth interlayer interfaces. Additionally, for the interlayer interfacial shear strength of the specimens, the nozzle with a tooth angle of 135° shows a more favorable effect.

(4) Interlocking improves the bonding of the interlayer interface, increasing the strength of 3D printed concrete. Additionally, the interlayer interlocking 3D printed concrete exhibits a reduction in the anisotropic coefficient (I_a) of about 13.7–25.5 %, and the anisotropy is significantly weakened.

CRediT authorship contribution statement

Youbao Jiang: Writing – review & editing, Supervision, Methodology, Investigation, Funding acquisition, Conceptualization. **Pengxiang Gao:** Writing – original draft, Validation, Investigation. **Sondipon Adhikari:** Writing – review & editing, Supervision. **Xiaofei Yao:** Resources, Project administration. **Hao Zhou:** Resources, Project administration. **Yan Liu:** Project administration.

Declaration of Competing Interest

The authors declare that they have no known competing financial interests or personal relationships that could have appeared to influence the work reported in this paper.

Acknowledgments

This research was funded by the National Natural Science Foundation Program of China (Grant No. 52378126), and the Open Fund of Engineering Research Center of Catastrophic Prophylaxis and Treatment of Road & Traffic Safety of Ministry of Education (Changsha University of Science & Technology), (Grant No. kfj230504).

Data availability

Data will be made available on request.

References

[1] Y. Jiang, X. Zhang, M. Beer, H. Zhou, Y. Leng, An efficient method for reliability-based design optimization of structures under random excitation by mapping between reliability and operator norm, Reliab. Eng. Syst. Saf. 245 (2024) 109972, https://doi.org/10.1016/j.ress.2024.109972.

[2] G. Ma, R. Buswell, W.R. Leal da Silva, L. Wang, J. Xu, S.Z. Jones, Technology readiness: a global snapshot of 3D concrete printing and the frontiers for development, Cem. Concr. Res. 156 (2022) 106774, https://doi.org/10.1016/j.cemconres.2022.106774.

[3] J. Ye, C. Cui, J. Yu, K. Yu, F. Dong, Effect of polyethylene fiber content on workability and mechanical-anisotropic properties of 3D printed ultra-high ductile concrete, Constr. Build. Mater. 281 (2021) 122586, https://doi.org/10.1016/j.conbuildmat.2021.122586.

[4] B. Panda, C. Unluer, M.J. Tan, Extrusion and rheology characterization of geopolymer nanocomposites used in 3D printing, Compos. Part B Eng. 176 (2019) 107290, https://doi.org/10.1016/j.compositesb.2019.107290.

[5] M.T. Mollah, R. Comminal, M.P. Serdeczny, D.B. Pedersen, J. Spangenberg, Stability and deformations of deposited layers in material extrusion additive manufacturing, Addit. Manuf. 46 (2021) 102193, https://doi.org/10.1016/j.addma.2021.102193.

[6] Q. Wan, L. Wang, G. Ma, Continuous and adaptable printing path based on transfinite mapping for 3D concrete printing, Autom. Constr. 142 (2022) 104471, https://doi.org/10.1016/j.autcon.2022.104471.

[7] Y. Li, H. Wu, X. Xie, L. Zhang, P.F. Yuan, Y.M. Xie, FloatArch: a cable-supported, unreinforced, and re-assemblable 3D-printed concrete structure designed using multi-material topology optimization, Addit. Manuf. 81 (2024) 104012, https://doi.org/10.1016/j.addma.2024.104012.

[8] K. Liu, K. Takasu, J. Jiang, K. Zu, W. Gao, Mechanical properties of 3D printed concrete components: a review, Dev. Built Environ. 16 (2023) 100292, https://doi.org/10.1016/j.dibe.2023.100292.

[9] S. Lim, R.A. Buswell, P.J. Valentine, D. Piker, S.A. Austin, X. De Kestelier, Modelling curved-layered printing paths for fabricating large-scale construction components, Addit. Manuf. 12 (2016) 216–230, https://doi.org/10.1016/j.addma.2016.06.004.

[10] A. Lin, A. Goel, D.H.A. Wong, C. Yeo, J. Chung, S.D. Pang, C.-H. Wang, H. Taylor, H.W. Kua, Compressive load-dominated concrete structures for customized 3D-printing fabrication, Autom. Constr. 141 (2022) 104467, https://doi.org/10.1016/j.autcon.2022.104467.

[11] Y. Wang, L.-c Qiu, Y.-y Hu, S.-g Chen, Y. Liu, Influential factors on mechanical properties and microscopic characteristics of underwater 3D printing concrete, J. Build. Eng. 77 (2023) 107571, https://doi.org/10.1016/j.jobe.2023.107571.

[12] K. Nakase, K. Hashimoto, T. Sugiyama, K. Kono, Influence of print paths on mechanical properties and fracture propagation of 3D printed concrete, Constr. Build. Mater. 438 (2024) 137019, https://doi.org/10.1016/j.conbuildmat.2024.137019.

[13] E. Secrieru, W. Mohamed, S. Fataei, V. Mechtcherine, Assessment and prediction of concrete flow and pumping pressure in pipeline, Cem. Concr. Compos. 107 (2020) 1–13, https://doi.org/10.1016/j.cemconcomp.2019.103495.

[14] T. Ding, J. Xiao, S. Zou, X. Zhou, Anisotropic behavior in bending of 3D printed concrete reinforced with fibers, Compos. Struct. 254 (2020) 112808, https://doi.org/10.1016/j.compstruct.2020.112808.

[15] J.G. Sanjayan, B. Nematollahi, M. Xia, T. Marchment, Effect of surface moisture on inter-layer strength of 3D printed concrete, Constr. Build. Mater. 172 (2018) 468–475, https://doi.org/10.1016/j.conbuildmat.2018.03.232.

[16] R.J.M. Wolfs, F.P. Bos, T.A.M. Salet, Hardened properties of 3D printed concrete: the influence of process parameters on interlayer adhesion, Cem. Concr. Res. 119 (2019) 132–140, https://doi.org/10.1016/j.cemconres.2019.02.017.

[17] J. Xiao, H. Liu, T. Ding, Finite element analysis on the anisotropic behavior of 3D printed concrete under compression and flexure, Addit. Manuf. 39 (2021) 101712, https://doi.org/10.1016/j.addma.2020.101712.

[18] T. Ding, J. Xiao, S. Zou, Y. Wang, Hardened properties of layered 3D printed concrete with recycled sand, Cem. Concr. Compos. 113 (2020) 103724, https://doi.org/10.1016/j.cemconcomp.2020.103724.

[19] Z. Deng, Z. Jia, C. Zhang, Z. Wang, L. Jia, L. Ma, X. Wang, Y. Zhang, 3D printing lightweight aggregate concrete prepared with shell-packing-aggregate method - Printability, mechanical properties and pore structure, J. Build. Eng. 62 (2022) 105404, https://doi.org/10.1016/j.jobe.2022.105404.

[20] Q. Jiang, Q. Liu, S. Wu, H. Zheng, W. Sun, Modification effect of nanosilica and polypropylene fiber for extrusion-based 3D printing concrete: printability and mechanical anisotropy, Addit. Manuf. 56 (2022) 102944, https://doi.org/10.1016/j.addma.2022.102944.

[21] P. Shakor, S. Nejadi, S. Sutjipto, G. Paul, N. Gowripalan, Effects of deposition velocity in the presence/absence of E6-glass fibre on extrusion-based 3D printed mortar, Addit. Manuf. 32 (2020) 101069, https://doi.org/10.1016/j.addma.2020.101069.

[22] Z. Jia, L. Kong, L. Jia, L. Ma, Y. Chen, Y. Zhang, Printability and mechanical properties of 3D printing ultra-high performance concrete incorporating limestone powder, Constr. Build. Mater. 426 (2024) 136195, https://doi.org/10.1016/j.conbuildmat.2024.136195.

[23] B. Panda, S.C. Paul, N.A.N. Mohamed, Y.W.D. Tay, M.J. Tan, Measurement of tensile bond strength of 3D printed geopolymer mortar, Measurement 113 (2018) 108–116, https://doi.org/10.1016/j.measurement.2017.08.051.

[24] B. Sun, R. Dominicus, E. Dong, P. Li, Z. Ye, W. Wang, Predicting the strength development of 3D printed concrete considering the synergistic effect of curing temperature and humidity: from perspective of modified maturity model, Constr. Build. Mater. 427 (2024) 136291, https://doi.org/10.1016/j.conbuildmat.2024.136291.

[25] L. Xia, G. Ma, F. Wang, G. Bai, Y.M. Xie, W. Xu, J. Xiao, Globally continuous hybrid path for extrusion-based additive manufacturing, Autom. Constr. 137 (2022) 104175, https://doi.org/10.1016/j.autcon.2022.104175.

[26] J. Xu, L. Ding, L. Cai, L. Zhang, H. Luo, W. Qin, Volume-forming 3D concrete printing using a variable-size square nozzle, Autom. Constr. 104 (2019) 95–106, https://doi.org/10.1016/j.autcon.2019.03.008.

[27] P. Shakor, S. Nejadi, G. Paul, A study into the effect of different nozzles shapes and fibre-reinforcement in 3D printed mortar, Materials 12 (10) (2019) 1708, https://doi.org/10.3390/ma12101708.

[28] W. McGee, T. Ng, K. Yu, V. Li, Extrusion nozzle shaping for improved 3DP of engineered cementitious composites (ECC/SHCC), Second RILEM Int. Conf. Concr. Digit. Fabr. (2020) 916–925, https://doi.org/10.1007/978-3-030-49916-789.

[29] R. Xin, F. Jia, M.A.R. Hamid, R. Ma, Z. Lu, Experimental study on the in-plane seismic performance of fully grouted interlocking block walls, J. Build. Eng. 97 (2024) 110851, https://doi.org/10.1016/j.jobe.2024.110851.

[30] S. Khandelwal, T. Siegmund, R.J. Cipra, J.S. Bolton, Adaptive mechanical properties of topologically interlocking material systems, Smart Mater. Struct. 24 (4) (2015) 045037, https://doi.org/10.1088/0964-1726/24/4/045037.

[31] J. Tian, X. Wu, J. Yuan, X. Tan, L. Wei, W. Zhang, P. Yu, Investigation on shear properties and mechanical model of FRP-ECC-concrete composite interface cast with 3D-printing pre-grooves, Structures 64 (2024) 106582, https://doi.org/10.1016/j.istruc.2024.106582.

[32] B. Zareiyan, B. Khoshnevis, Effects of interlocking on interlayer adhesion and strength of structures in 3D printing of concrete, Autom. Constr. 83 (2017) 212–221, https://doi.org/10.1016/j.autcon.2017.08.019.

[33] L. He, H. Li, W.T. Chow, B. Zeng, Y. Qian, Increasing the interlayer strength of 3D printed concrete with tooth-like interface: an experimental and theoretical investigation, Mater. Des. 223 (2022) 111117, https://doi.org/10.1016/j.matdes.2022.111117.

[34] L. Wang, Y. Liu, Y. Yang, Y. Li, M. Bai, Bonding performance of 3D printing concrete with self-locking interfaces exposed to compression–shear and compression–splitting stresses, Addit. Manuf. 42 (2021) 101992, https://doi.org/10.1016/j.addma.2021.101992.

[35] M. Qiu, Y. Sun, Y. Qian, Interfacial bonding performance of 3D-printed ultra-high performance strain-hardening cementitious composites (UHP-SHCC) and cast normal concrete, J. Build. Eng. 82 (2024) 108268, https://doi.org/10.1016/j.jobe.2023.108268.

[36] J. Van Der Putten, G. De Schutter, K. Tittelboom, Surface modification as a technique to improve inter-layer bonding strength in 3D printed cementitious materials, RILEM Tech. Lett. 4 (2019) 33–38, https://doi.org/10.21809/rilemtechlett.2019.84.

[37] L. Yang, S.M.E. Sepasgozar, S. Shirowzhan, A. Kashani, D. Edwards, Nozzle criteria for enhancing extrudability, buildability and interlayer bonding in 3D printing concrete, Autom. Constr. 146 (2023) 104671, https://doi.org/10.1016/j.autcon.2022.104671.

[38] O. Kontovourkis, G. Tryfonos, Robotic 3D clay printing of prefabricated non-conventional wall components based on a parametric-integrated design, Autom. Constr. 110 (2020) 103005, https://doi.org/10.1016/j.autcon.2019.103005.

[39] Z. Liu, M. Li, Y.W.D. Tay, Y. Weng, T.N. Wong, M.J. Tan, Rotation nozzle and numerical simulation of mass distribution at corners in 3D cementitious material printing, Addit. Manuf. 34 (2020) 101190, https://doi.org/10.1016/j.addma.2020.101190.

[40] K. El Cheikh, S. Rémond, N. Khalil, G. Aouad, Numerical and experimental studies of aggregate blocking in mortar extrusion, Constr. Build. Mater. 145 (2017) 452–463, https://doi.org/10.1016/j.conbuildmat.2017.04.032.

[41] Cement (SAC/TC 184) (2005). Test method for fluidity of cement mortar. GB/T 2419-2005. General Administration of Quality Supervision, Inspection and Quarantine of the People's Republic of China; Standardization Administration of the People's Republic of China. [In Chinese].

[42] Comminal, R., da Silva, W.R.L., Andersen, T.J., Stang, H., & Spangenberg, J. (2020). Influence of Processing Parameters on the Layer Geometry in 3D Concrete Printing: Experiments and Modelling. Second RILEM International Conference on Concrete and Digital Fabrication, Cham, 28, 852-862.

[43] H. He, Y. Jiang, Y. Deng, L. Peng, Y. Zhang, J. Wen, Experimental study on segmental forming of 3D printing prefabricated, J. Chang. Univ. Sci. Technol. Nat. Sci. 19 (4) (2022) 47–54.

[44] Y. Jiang, J. Hu, H. Zhou, H. He, J. Wen, Continuous printed height of 3D printing concrete circular tube with equiangular movements of starting point, J. Build. Struct. 43 (09) (2021) 222–231.

[45] Ministry of Housing and Urban-Rural Development, PRC, GB/T50081-2019. Standards for test methods of physical and mechanical properties of concrete, China Architecture & Building Press, Beijing, 2019.

[46] China Concrete & Cement-based Products Association, T/CCPA 33—2022/ T/CBMF 183—2022. Test methods for basic mechanical properties of 3D printed concrete, 2022.

[47] S. Luo, W. Li, Y. Cai, K. Zhang, Effects of carbonated recycled sand on the interfacial bonding performance of 3D printed cement-based material, J. Build. Eng. (2024) 111551, https://doi.org/10.1016/j.jobe.2024.111551.

[48] M. Chilwesa, F. Minelli, A. Reggia, G. Plizzari, Evaluating the shear bond strength between old and new concrete through a new test method, Mag. Concr. Res. 69 (9) (2017) 425–435, https://doi.org/10.1680/jmacr.16.00327.

[49] D.S. Santos, P.M.D. Santos, D. Dias-da-Costa, Effect of surface preparation and bonding agent on the concrete-to-concrete interface strength, Constr. Build. Mater. 37 (2012) 102–110, https://doi.org/10.1016/j.conbuildmat.2012.07.028.

[50] H. Wang, J. Shao, J. Zhang, D. Zou, X. Sun, Bond shear performances and constitutive model of interfaces between vertical and horizontal filaments of 3D printed concrete, Constr. Build. Mater. 316 (2022) 125819, https://doi.org/10.1016/j.conbuildmat.2021.125819.

[51] H. Beushausen, M. Alexander, Bond strength development between concretes of different ages, MAG. Concr. Res. 60 (2008) 65–74, https://doi.org/10.1680/macr.2007.00108.

[52] X. Wu, J. He, J. Tian, X. Tan, S. Hu, Y. Zheng, W.-W. Wang, W. Zhang, Shear behaviors of engineered cementitious composites to seawater sea-sand concrete (ECC-to-SSSC) interfaces cast using 3D-printed pre-grooving formwork: mechanical properties, characterization, and life-cycle assessment, J. Build. Eng. 78 (2023) 107636, https://doi.org/10.1016/j.jobe.2023.107636.

[53] T. Hua, A. Lin, W.J.D. Poh, Charlene, D.H.A. Wong, H. Zhang, Y.Z. Chan, W. Liu, L. Zhao, 3D-printed concrete shear keys: design and experimental study, Dev. Built Environ. 15 (2023) 100180, https://doi.org/10.1016/j.dibe.2023.100180.

[54] A. Yuan, C. Yang, J. Wang, L. Chen, R. Lu, Shear behavior of epoxy resin joints in precast concrete segmental bridges, J. Bridge Eng. 24 (4) (2019) 04019009, https://doi.org/10.1061/(ASCE)BE.1943-5592.0001362.

[55] G. Ma, Z. Li, L. Wang, F. Wang, J. Sanjayan, Mechanical anisotropy of aligned fiber reinforced composite for extrusion-based 3D printing, Constr. Build. Mater. 202 (2019) 770–783, https://doi.org/10.1016/j.conbuildmat.2019.01.008.